TVD Flux Vector Splitting Algorithms Applied to the Solution of the Euler and Navier-Stokes Equations in Three-Dimensions – Part II

EDISSON SÁVIO DE GÓES MACIEL
IEA- Aeronautical Engineering Division
ITA – Aeronautical Technological Institute
Praça Mal. Eduardo Gomes, 50 – Vila das Acácias – São José dos Campos – SP – 12228-900
BRAZIL
edissonsavio@yahoo.com.br

Abstract: - In the present work, the Steger and Warming, the Van Leer, the Liou and Steffen Jr. and the Radespiel and Kroll schemes are implemented, on a finite volume context and using a structured spatial discretization, to solve the Euler and the Navier-Stokes equations in three-dimensions. A MUSCL ("Monotone Upstream-centered Schemes for Conservation Laws") approach is implemented in these schemes aiming to obtain second order spatial accuracy and TVD ("Total Variation Diminishing") high resolution properties. An implicit formulation is employed to the Euler equations, whereas the Navier-Stokes equations use an explicit formulation. The algebraic turbulence models of Cebeci and Smith and of Baldwin and Lomax are implemented. The problems of the supersonic flow along a compression corner (inviscid case), and of the supersonic flow along a ramp (viscous case) are solved. The results have demonstrated that the most severe and most accurate results are obtained with the Liou and Steffen Jr. TVD scheme. The first paper of this work treats the inviscid and laminar viscous results. In this paper, the second of this series, the turbulent results are presented.

Key-Words: - Steger and Warming algorithm, Van Leer algorithm, Liou and Steffen Jr. algorithm, Radespiel and Kroll algorithm, TVD high resolution schemes, Turbulence models, Euler and Navier-Stokes equations, Three-Dimensions.

1 Introduction

Conventional non-upwind algorithms have been used extensively to solve a wide variety of problems ([1-2]). Conventional algorithms are somewhat unreliable in the sense that for every different problem (and sometimes, every different case in the same class of problems) artificial dissipation terms must be specially tuned and judicially chosen for convergence. Also, complex problems with shocks and steep compression and expansion gradients may defy solution altogether.

Upwind schemes are in general more robust but are also more involved in their derivation and application. Some upwind schemes that have been applied to the Euler equations are: [3-7]. Some comments about these methods are reported in [8]. The interesting reader is encouraged to read the first part of this work ([8]).

Second order spatial accuracy can be achieved by introducing more upwind points or cells in the schemes. It has been noted that the projection stage, whereby the solution is projected in each cell face $(i-\frac{1}{2},i+\frac{1}{2})$ on piecewise constant states, is the cause of the first order space accuracy of the Godunov schemes ([9]). Hence, it is sufficient to modify the first projection stage without modifying the Riemann solver, in order to generate higher spatial approximations. The state variables at the interfaces are thereby obtained from an extrapolation between neighboring cell averages. This method for the generation of second order upwind schemes based on variable extrapolation is often referred to in the literature as the MUSCL ("Monotone Upstream-centered Schemes for Conservation Laws") approach. More details about this method are found in [8-9]

Traditionally, implicit numerical methods have been praised for their improved stability and condemned for their large arithmetic operation counts ([10]). On the one hand, the slow convergence rate of explicit methods become they so unattractive to the solution of steady state problems due to the large number of iterations required to convergence, in spite of the reduced number of operation counts per time step in comparison with their implicit counterparts. Such problem is resulting from the limited stability region which such methods are subjected (the Courant condition). On the other hand, implicit schemes guarantee a larger stability region, which allows the use of CFL numbers above 1.0, and fast convergence to steady state conditions.

Undoubtedly, the most significant efficiency achievement for multidimensional implicit methods was the introduction of the Alternating Direction Implicit (ADI) algorithms by [11-13], and fractional step algorithms by [14]. To more details of the ADI method, the reader is encouraged to read [8, 11-13]

There is a practical necessity in the aeronautical industry and in other fields of the capability of calculating separated turbulent compressible flows. With the available numerical methods, researches seem able to analyze several separated flows, three-dimensional in general, if an appropriated turbulence model is employed. Simple methods as the algebraic turbulence models of [15-16] supply satisfactory results with low computational cost and allow that the main features of the turbulent flow be detected.

[17] performed a comparison between the [18] and [19] schemes implemented coupled with the [15] and [16] models to accomplish turbulent flow simulations in three-dimensions. The Navier-Stokes equations in conservative and integral forms were solved, employing a finite volume formulation and a structured spatial discretization. The [18] scheme is a predictor/corrector method which performs coupled time and space discretizations, whereas the [19] algorithm is a symmetrical scheme and its time discretization is performed by a Runge-Kutta method. Both schemes are second order accurate in space and time and require artificial dissipation to guarantee stability. The steady state problem of the supersonic turbulent flow along a ramp was studied. The results have demonstrated that both turbulence models predicted appropriately the boundary layer separation region formed at the compression corner, reducing, however, its extension in relation to the laminar solution, as expected.

In the present work, the [4-7] schemes are implemented, on a finite volume context and using a structured spatial discretization, to solve the Euler and the laminar/turbulent Navier-Stokes equations in the three-dimensional space. All schemes are flux vector splitting ones and in their original implementations are first order accurate. A MUSCL approach is implemented in these schemes aiming to obtain second order spatial accuracy. The Van Leer, the Van Albada and the Minmod nonlinear limiters are employed to guarantee such accuracy and TVD high resolution properties. These flux vector splitting schemes employ approximate factorizations in ADI form to solve implicitly the Euler equations. To solve the laminar/turbulent Navier-Stokes equations, an explicit formulation based on a dimensional splitting procedure is employed. All schemes are first order accurate in time in their implicit and explicit versions. Turbulence is taken into account considering two algebraic models, namely: [15-16]. The algorithms are accelerated to the steady state solution using a spatially variable time step, which has demonstrated effective gains in terms of convergence rate ([20-21]). All four schemes are applied to the solution of the physical problems of the supersonic flow along a compression corner, in the inviscid case, and of the supersonic flow along a ramp, in the laminar and turbulent cases. The results have demonstrated that the most severe and most accurate results are obtained with the [6] TVD high resolution scheme. The inviscid and laminar viscous results are presented in the first part of this work [8]. Turbulent results are presented in this paper.

The main contribution of this work to the CFD (Computational Fluid Dynamics) community is the extension of the TVD high resolution algorithms of [4-7] to the three-dimensional space, following a finite volume formulation, and their implementation coupled with two different algebraic turbulence models to simulate viscous turbulent flows, which characterizes an original contribution in the field of high resolution structured numerical algorithms. The implicit implementation in three-dimensions of these algorithms is also a meaningful contribution.

2 Results

Tests were performed in a microcomputer with processor AMD SEMPRON (tm) 2600+, 1.83GHz of clock, and 512 Mbytes of RAM memory. As the interest of this work is steady state problems, one needs to define a criterion which guarantees that such condition was reached. The criterion adopted in this work was to consider a reduction of 3 orders in the magnitude of the maximum residual in the domain, a typical criterion in the CFD community. The residual to each cell was defined as the numerical value obtained from the discretized conservation equations. As there are five conservation equations to each cell, the maximum value obtained from these equations is defined as the residual of this cell. Thus, this residual is compared with the residual of the others cells, calculated of the same way, to define the maximum residual in the domain. The configuration upstream and the configuration longitudinal plane angles were set equal to 0.0°. All pressure distributions were determined at the plane corresponding to k = KMAX/2, where “KMAX” is the maximum number of points in the z direction, and j = 1, corresponding to the configuration wall.

The physical problem studied in the viscous turbulent simulations is the flow along a ramp. This problem is a supersonic flow hitting a ramp with 20° of inclination. It generates a shock and an expansion fan. The freestream Mach number adopted as initial condition to this simulation was 3.0, characterizing a moderate supersonic flow. The Reynolds number was estimated to be 2.419×10^5 at a flight altitude of 20,000m and l = 0.0437m, based on the work of [22]. To this Mach number and Reynolds number, a separated flow is formed at the ramp wall, with the formation of a circulation bubble. This behaviour is observed in all solutions of all schemes. To details of the ramp configuration and mesh, see [8].

2.1 Turbulent Case – [15] Model

Figures 1 to 6 exhibit the pressure contours and the streamlines of the velocity vector field generated by the [4] TVD scheme in its three variants, namely: VL (Van Leer), VA (Van Albada) and Min (Minmod), using the [15] turbulence model. Figures 1 and 2 show the pressure contours and the streamlines, respectively, obtained by the [4] TVD scheme using VL limiter; Figures 3 and 4 show the pressure contours and the streamlines, respectively, obtained by the [4] TVD scheme using VA limiter; and Figures 5 and 6 show the pressure contours and the streamlines, respectively, obtained by the [4] TVD scheme using Min limiter. The [4] TVD scheme using VL limiter yields the most severe pressure field, which characterizes the most conservative solution, involving the variants of this scheme. Good symmetry and homogeneity properties at the k planes are observed in all solutions. The shock wave is well captured. The circulation bubble is also well captured by the three limiters.

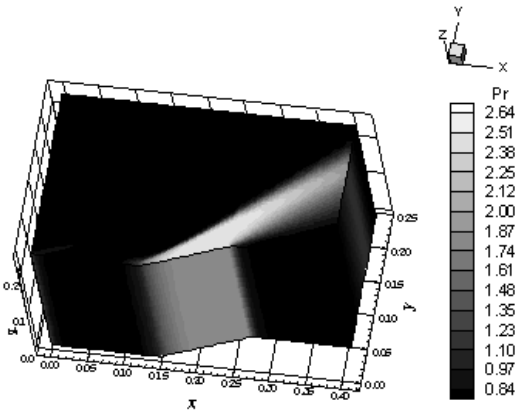

Figure 1. Pressure contours ([4]-VL).

Figure 7 exhibits the wall pressure distribution obtained by all three variants of the [4] TVD scheme using the [15] turbulence model. They are compared with the oblique shock wave and the expansion wave Prandtl-Meyer theory results. All schemes detect ahead of the ramp beginning a weaker shock, which is formed due to the increase of the boundary layer thickness in this region, because of the flow separation, and the formation of the circulation bubble.

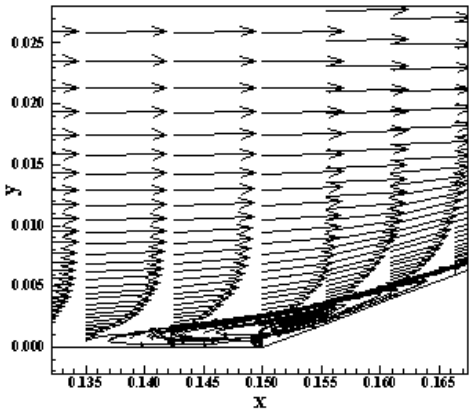

Figure 2. Streamlines and circulation bubble ([4]-VL).

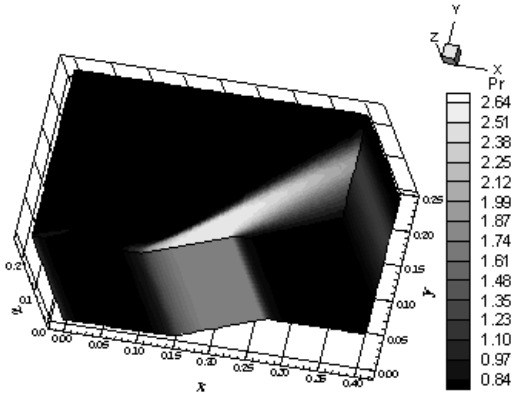

Figure 3. Pressure contours ([4]-VA).

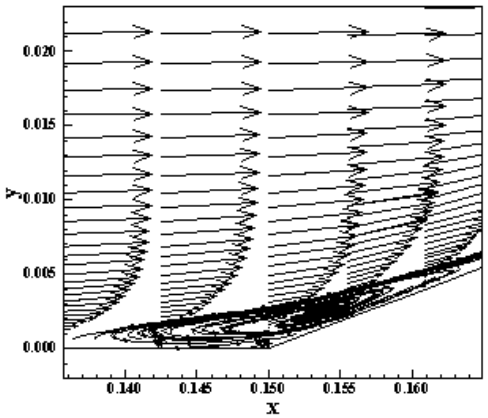

Figure 4. Streamlines and circulation bubble ([4]-VA).

As can be observed, these weaker shocks are less pronounced than the respective ones obtained in the laminar case because the effect of the turbulence model is to stabilize the boundary layer in presence of adverse pressure gradient, reducing, hence, the extension of the separation region.

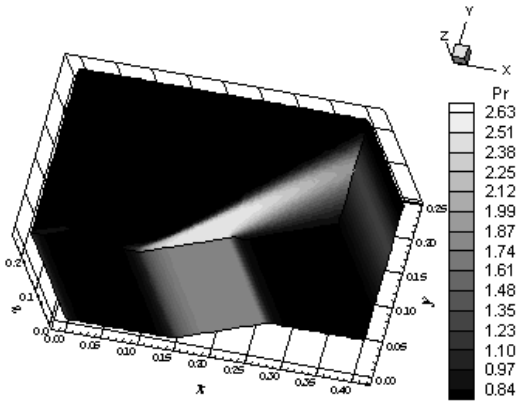

Figure 5. Pressure contours ([4]-Min).

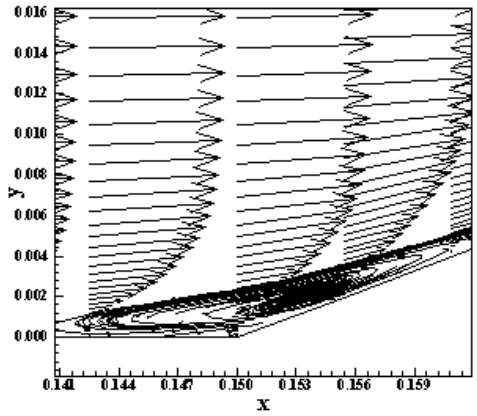

Figure 6. Streamlines and circulation bubble ([4]-Min).

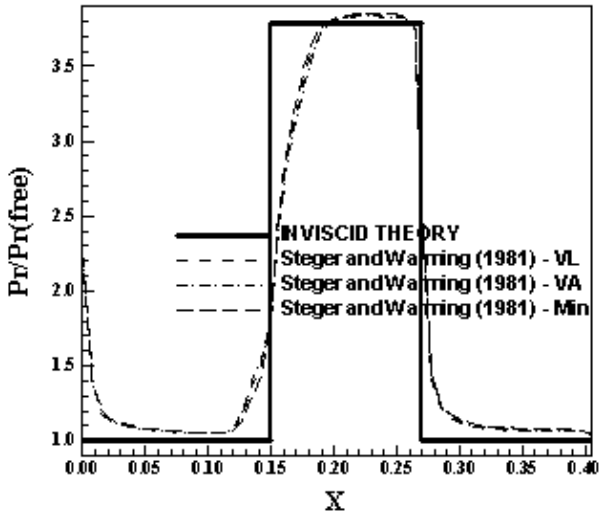

Figure 7. Wall pressure distributions ([4]-CS).

All three variants of the [4] TVD scheme slightly over-predict the shock plateau, presenting a small divergence in relation to the inviscid solution. The pressure recovery at the end of the expansion fan is reasonable detected by all three variants of the [4] TVD scheme, although the laminar solution presents better capture of the pressure at the end of the expansion (see [8] for comparison).

Table 1 shows the detachment and reattachment points obtained by the three limiters studied with the [4] scheme using the [15] turbulence model. The [4] scheme using Min limiter and the [15] model presents the minimum extent of the separation region. This region of separated flow is less extent than the respective one of the laminar results, as seen in [8].

Table 1. Flow separation detachment and reattachment points ([4]-Turbulent).

Scheme	Detachment (m)	Reattachment (m)
[4]-VL	0.1350	0.1664
[4]-VA	0.1350	0.1664
[4]-Min	0.1425	0.1609

One way to quantitatively verify if the solutions generated by each variant of the [4] TVD scheme are satisfactory consists in determining the shock angle of the oblique shock wave, β, measured in relation to the initial direction of the flow field. [23] (pages 352 and 353) presents a diagram with values of the shock angle, β, to oblique shock waves. The value of this angle is determined as function of the freestream Mach number and of the deflection angle of the flow after the shock wave, ϕ. To the ramp problem, $\phi = 20^{o}$ (ramp inclination angle) and the freestream Mach number is 3.0, resulting from this diagram a value to β equals to 37.7^{o}.

Table 2. Shock angle of the oblique shock wave at the ramp and percentage error ([4]-Turbulent).

Scheme	β (°)	Error (%)
[4]-VL	38.4	1.86
[4]-VA	38.5	2.12
[4]-Min	39.2	3.98

Using a transfer in Figures 1, 3 and 5, considering the xy plane, it is possible to obtain the values of the shock angle of the oblique shock wave, β, to each variant of the [4] TVD scheme using the [15] turbulence model, as w

ell the respective errors, shown in Tab. 2. As can be observed, the best variant was the [4] TVD scheme using VL limiter with the [15] model, with a percentage error of 1.86%.

As conclusion of the study analyzing the [4] TVD scheme in its three variants using the [15] model, the best variant is the [4] TVD scheme using VL limiter due to better accuracy than the others limiters in the determination of the shock angle.

Figures 8 to 11 exhibit the pressure contours and the streamlines of the velocity vector field generated by the [5] TVD scheme in its two variants, namely: VA and Min, using the [15] turbulence model. The VL limiter did not present converged results. Figures 8 and 9 show the pressure contours and the streamlines, respectively, obtained by the [5] TVD scheme using VA limiter; and Figures 10 and 11 show the pressure contours and the streamlines, respectively, obtained by the [5] TVD scheme using Min limiter. It is possible to highlight the circulation bubble that is formed in both solutions.

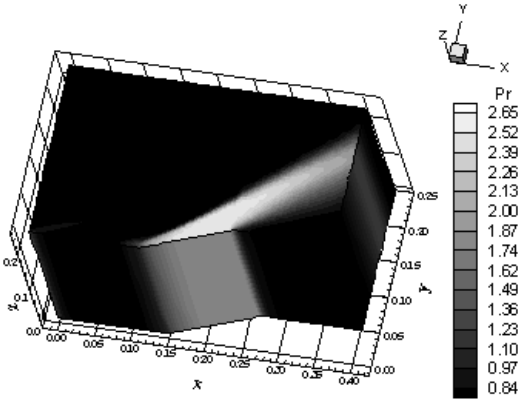

Figure 8. Pressure contours ([5]-VA).

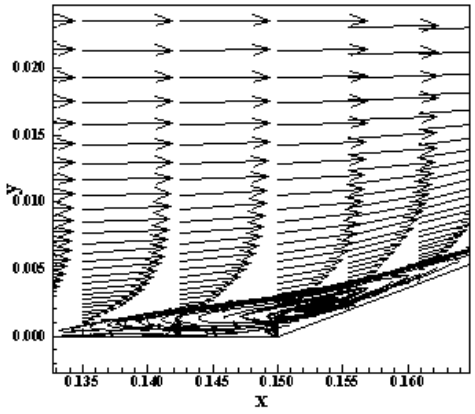

Figure 9. Streamlines and circulation bubble ([5]-VA).

Figure 12 exhibits the wall pressure distribution obtained by the two variants of the [5] TVD scheme using the [15] turbulence model. They are compared with the oblique shock wave and the expansion wave Prandtl-Meyer theory results.

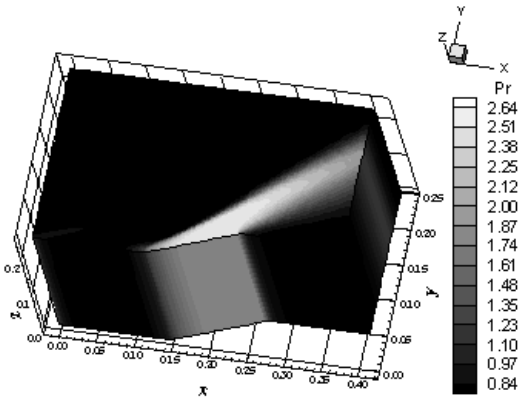

Figure 10. Pressure contours ([5]-Min).

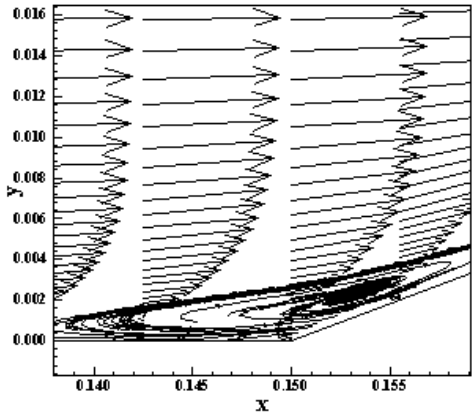

Figure 11. Streamlines and circulation bubble ([5]-Min).

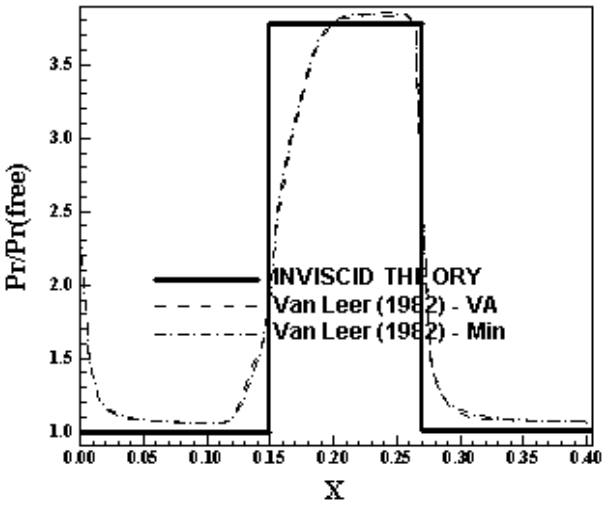

Figure 12. Wall pressure distributions ([5]-CS).

The [5] TVD scheme using VA limiter yields more severe pressure field than the Min limiter, which characterizes a more conservative solution, involving these two variants of this scheme. Good

symmetry and homogeneity properties at the k planes are observed in all solutions. The shock wave is well captured. The circulation bubble is also well captured by the two limiters. All schemes detect ahead of the ramp beginning a weaker shock, which is formed due to the increase of the boundary layer thickness in this region, because of the flow separation, and the formation of the circulation bubble. As can be observed, these weaker shocks are less pronounced than the respective ones obtained in the laminar case because the effect of the turbulence model is to stabilize the boundary layer in presence of adverse pressure gradient, reducing, hence, the extension of the separation region. Both variants of the [5] TVD scheme slightly over-predict the shock plateau, presenting a small divergence in relation to the inviscid solution. The pressure recovery at the end of the expansion fan is reasonable detected by both variants of the [5] TVD scheme, although the laminar solution presents better capture of the pressure at the end of the expansion (see [8]).

Table 3 shows the detachment and reattachment points obtained by the two limiters studied with the [5] TVD scheme using the [15] turbulence model. The [5] TVD scheme using Min limiter and the [15] model presents the minimum extent of the separation region. This region of separated flow is less extent than the respective one of the laminar results, as was recognized in those studies.

Table 3. Flow separation detachment and reattachment points ([5]-Turbulent).

Scheme	Detachment (m)	Reattachment (m)
[5]-VA	0.1350	0.1664
[5]-Min	0.1350	0.1610

Table 4. Shock angle of the oblique shock wave at the ramp and percentage error ([5]-Turbulent).

Scheme	β (°)	Error (%)
[5]-VA	38.5	2.12
[5]-Min	39.0	3.45

Using a transfer in Figures 8 and 10, considering the xy plane, it is possible to obtain the values of the shock angle of the oblique shock wave, β, to each variant of the [5] TVD scheme using the [15] turbulence model, as well the respective errors, shown in Tab. 4. As can be observed, the best variant was the [5] TVD scheme using VA limiter with the [15] model, with a percentage error of 2.12%.

As conclusion of the study analyzing the [5] TVD scheme in its two variants using the [15] model, the best variant is the [5] TVD scheme using VA limiter due to better accuracy than the Min limiter in the determination of the shock angle.

Figures 13 to 18 exhibit the pressure contours and the streamlines of the velocity vector field generated by the [6] TVD scheme in its three variants, namely: VL, VA and Min, using the [15] turbulence model. Figures 13 and 14 show the pressure contours and the streamlines, respectively, obtained by the [6] TVD scheme using VL limiter; Figures 15 and 16 show the pressure contours and the streamlines, respectively, obtained by the [6] TVD scheme using VA limiter; and Figures 17 and 18 show the pressure contours and the streamlines, respectively, obtained by the [6] TVD scheme using Min limiter.

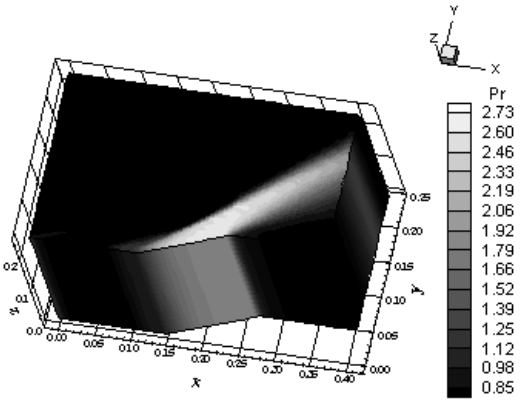

Figure 13. Pressure contours ([6]-VL).

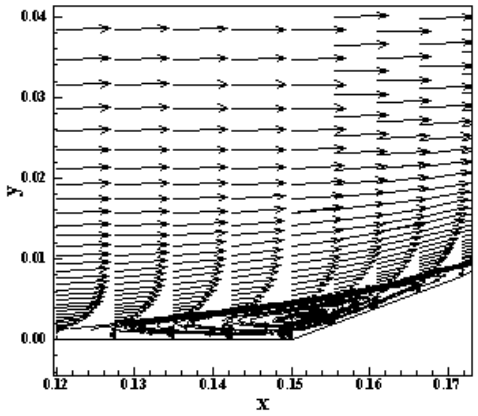

Figure 14. Streamlines and circulation bubble ([6]-VL).

The [6] TVD scheme using VA limiter yields the most severe pressure field, which characterizes the most conservative solution, involving the variants of this scheme. Good symmetry and homogeneity

properties at the k planes are observed in all solutions. The shock wave is well captured. The circulation bubble is also well captured by the three limiters.

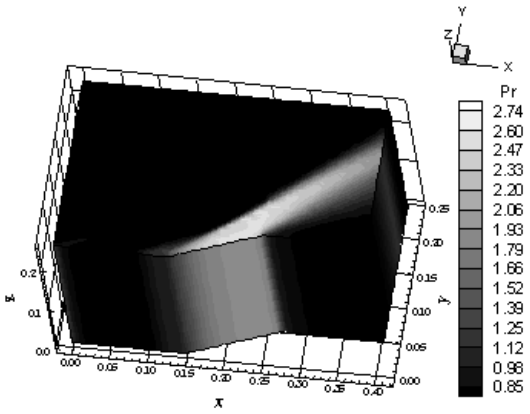

Figure 15. Pressure contours ([6]-VA).

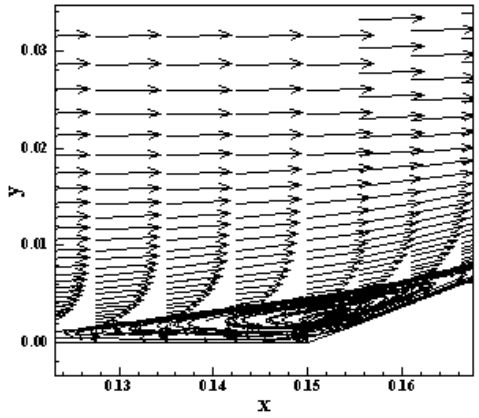

Figure 16. Streamlines and circulation bubble ([6]-VA).

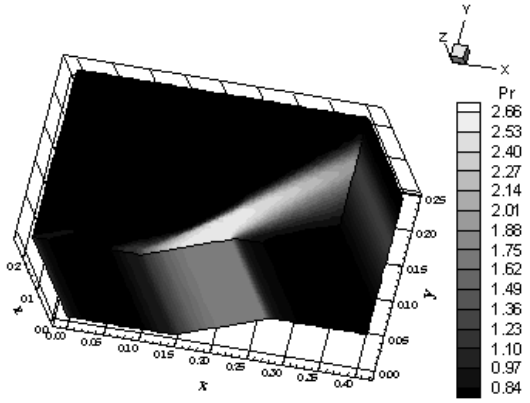

Figure 17. Pressure contours ([6]-Min).

Figure 19 exhibits the wall pressure distribution obtained by all three variants of the [6] TVD scheme using the [15] turbulence model. They are compared with the oblique shock wave and the expansion wave Prandtl-Meyer theory results.

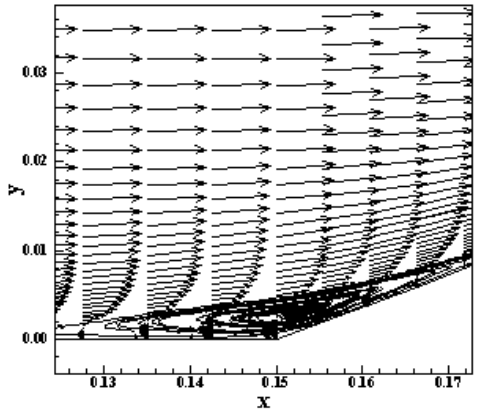

Figure 18. Streamlines and circulation bubble ([6]-Min).

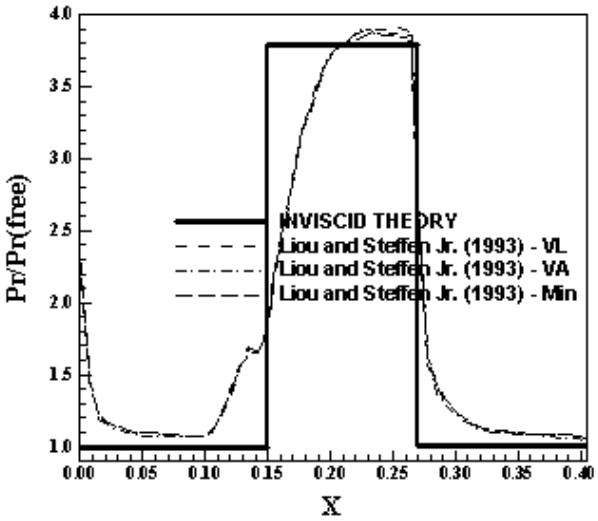

Figure 19. Wall pressure distributions ([6]-CS).

All schemes detect ahead of the ramp beginning a weaker shock, which is formed due to the increase of the boundary layer thickness in this region, because of the flow separation, and the formation of the circulation bubble. As can be observed, these weaker shocks are less pronounced than the respective ones obtained in the laminar case because the effect of the turbulence model is to stabilize the boundary layer in presence of adverse pressure gradient, reducing, hence, the extension of the separation region. All three variants of the [6] TVD scheme slightly over-predict the shock plateau, presenting a small divergence in relation to the inviscid solution. The pressure recovery at the end of the expansion fan is also reasonable detected by all three variants of the [6] TVD scheme, although the laminar solution presents better capture of the pressure at the end of the expansion.

Table 5 shows the detachment and reattachment points obtained by the three limiters studied with the [6] TVD scheme using the [15] turbulence model. The [6] TVD scheme using VA limiter and the [15] model presents the minimum extent of the separation region. This region of separated flow is less extent than the respective one of the laminar results, as was recognized in those studies.

Table 5. Flow separation detachment and reattachment points ([6]-Turbulent).

Scheme	Detachment (m)	Reattachment (m)
[6]-VL	0.1200	0.1772
[6]-VA	0.1200	0.1720
[6]-Min	0.1200	0.1772

Using a transfer in Figures 13, 15 and 17, considering the xy plane, it is possible to obtain the values of the shock angle of the oblique shock wave, β, to each variant of the [6] TVD scheme using the [15] turbulence model, as well the respective errors, shown in Tab. 6. As can be observed, the best variants were the [6] TVD scheme using VL and Min limiters with the [15] model, with a percentage error of 0.00%.

Table 6. Shock angle of the oblique shock wave at the ramp and percentage error ([6]-Turbulent).

Scheme	β (°)	Error (%)
[6]-VL	37.7	0.00
[6]-VA	37.9	0.53
[6]-Min	37.7	0.00

As conclusion of the study analyzing the [6] TVD scheme in its three variants using the [15] model, the best variants are the [6] TVD scheme using VL and Min limiters due to better accuracy in the determination of the shock angle.

Figures 20 to 25 exhibit the pressure contours and the streamlines of the velocity vector field generated by the [7] TVD scheme in its three variants, namely: VL, VA and Min, using the [15] turbulence model. Figures 20 and 21 show the pressure contours and the streamlines, respectively, obtained by the [8] TVD scheme using VL limiter; Figures 22 and 23 show the pressure contours and the streamlines, respectively, obtained by the [7] TVD scheme using VA limiter; and Figures 24 and 25 show the pressure contours and the streamlines, respectively, obtained by the [7] TVD scheme using Min limiter.

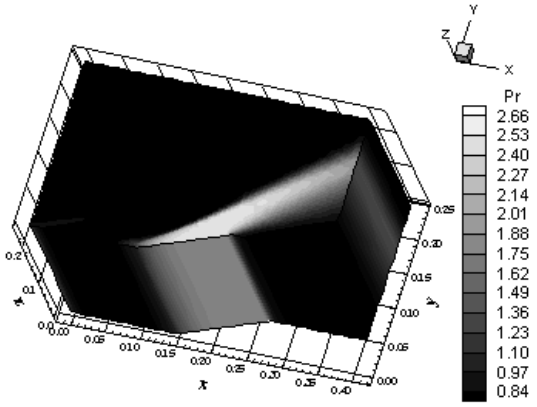

Figure 20. Pressure contours ([7]-VL).

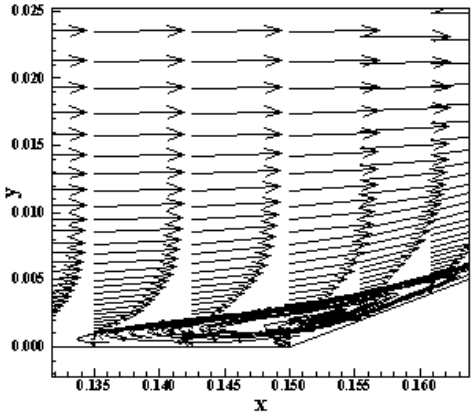

Figure 21. Streamlines and circulation bubble ([7]-VL).

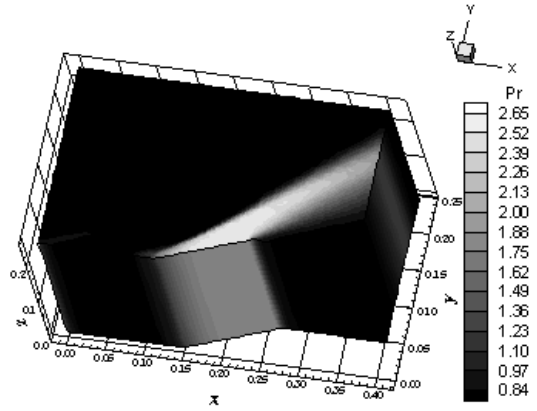

Figure 22. Pressure contours ([7]-VA).

The [7] TVD scheme using VL limiter yields the most severe pressure field, which characterizes the most conservative solution, involving the variants of this scheme. Good symmetry and homogeneity properties at the k planes are observed in all solutions. The shock wave is well captured. The circulation bubble is also well captured by the three limiters.

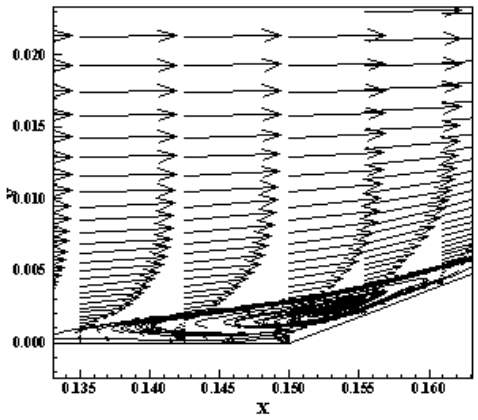

Figure 23. Streamlines and circulation bubble ([7]-VA).

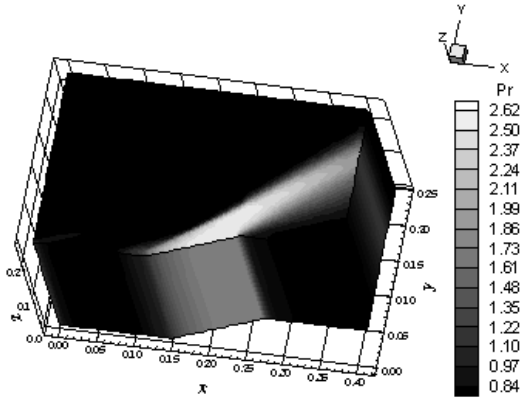

Figure 24. Pressure contours ([7]-Min).

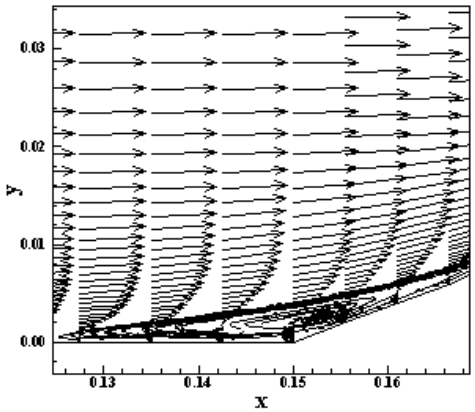

Figure 25. Streamlines and circulation bubble ([7]-Min).

Figure 26 exhibits the wall pressure distribution obtained by all three variants of the [7] TVD scheme using the [15] turbulence model. They are compared with the oblique shock wave and the expansion wave Prandtl-Meyer theory results. All schemes detect ahead of the ramp beginning a weaker shock. As can be observed, these weaker shocks are less pronounced than the respective ones obtained in the laminar case. All three variants of the [7] TVD scheme slightly over-predict the shock plateau, presenting a small divergence in relation to the inviscid solution. The pressure recovery at the end of the expansion fan is reasonable captured by all three variants of the [7] TVD scheme.

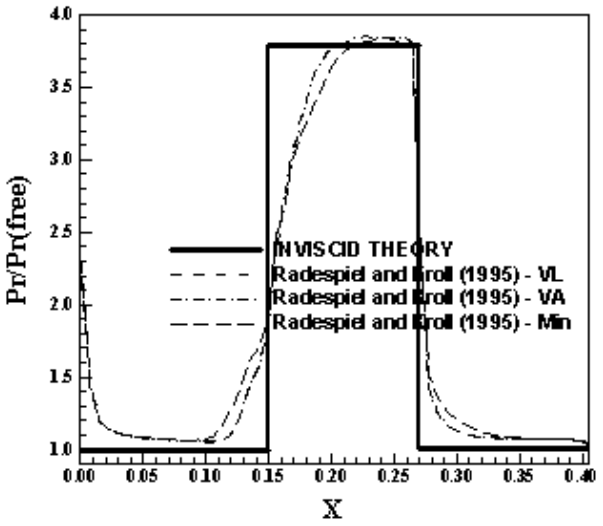

Figure 26. Wall pressure distributions ([7]-CS).

Table 7 shows the detachment and reattachment points obtained by the three limiters studied with the [7] TVD scheme using the [15] turbulence model. The [7] TVD scheme using VL limiter and the [15] model presents the minimum extent of the separation region. This region of separated flow is less extent than the respective one of the laminar results.

Table 7. Flow separation detachment and reattachment points ([7]-Turbulent).

Scheme	Detachment (m)	Reattachment (m)
[7]-VL	0.1350	0.1610
[7]-VA	0.1350	0.1664
[7]-Min	0.1275	0.1717

Using a transfer in Figures 20, 22 and 24, considering the xy plane, it is possible to obtain the values of the shock angle of the oblique shock wave, β, to each variant of the [7] TVD scheme using the [15] turbulence model, as well the respective errors, shown in Tab. 8. As can be observed, all three limiters employed with the [7] scheme using the [15] model present the same value to the shock angle, with a percentage error of 0.80%.

As conclusion of the study analyzing the [7] TVD scheme in its three variants using the [15]

model, the best variant is the [7] TVD scheme using VL limiter due to good accuracy in the determination of the shock angle and the prediction of a more severe pressure field.

Table 8. Shock angle of the oblique shock wave at the ramp and percentage error ([7]-Turbulent).

Scheme	β (°)	Error (%)
[7]-VL	38.0	0.80
[7]-VA	38.0	0.80
[7]-Min	38.0	0.80

As global conclusion, the most severe pressure field using the [15] model was obtained by the [6] scheme using VA limiter, as occurred in the laminar case. The best wall pressure distributions are obtained by the [7] TVD scheme in its variants. They present pressure plateau closer to the theoretical results than the others TVD schemes. The minimum extent of the separated flow region was detected by the [4] TVD scheme using Min limiter, as occurred in the laminar case.

Table 9. Shock angle of the oblique shock wave at the ramp and percentage error (Best Results – [15]).

Scheme	β (°)	Error (%)
[4]-VL	38.4	1.86
[5]-VA	38.5	2.12
[6]-VL	37.7	0.00
[6]-Min	37.7	0.00
[7]-VL	38.0	0.80
[7]-VA	38.0	0.80
[7]-Min	38.0	0.80

Table 9 presents the best values of the shock angle of the oblique shock wave obtained by each scheme. The best result of all schemes, detecting more precisely the value of the shock angle, is due to [6] TVD scheme using VL and Min limiters. As the [6] TVD scheme has presented the best value to the shock angle of the oblique shock wave with the VL and Min variants, the best scheme in this viscous turbulent simulation using the [15] model is due to the [6] scheme using VL and Min limiters, although the [7] in its variants capture better pressure distribution and the [4] TVD scheme using Min limiter detects the minimum region of separated flow.

2.2 Turbulent Case – [16] Model

Figures 27 to 32 exhibit the pressure contours and the streamlines of the velocity vector field generated by the [4] TVD scheme in its three variants, namely: VL, VA and Min, using the [16] turbulence model. Figures 27 and 28 show the pressure contours and the streamlines, respectively, obtained by the [4] TVD scheme using VL limiter; Figures 29 and 30 show the pressure contours and the streamlines, respectively, obtained by the [4] TVD scheme using VA limiter; and Figures 31 and 32 show the pressure contours and the streamlines, respectively, obtained by the [4] TVD scheme using Min limiter. The [4] TVD scheme using VL limiter yields the most severe pressure field, which characterizes the most conservative solution, involving the variants of this scheme. Good symmetry and homogeneity properties at the k planes are observed in all solutions. The shock wave is well captured. The circulation bubble is also well captured by the three limiters.

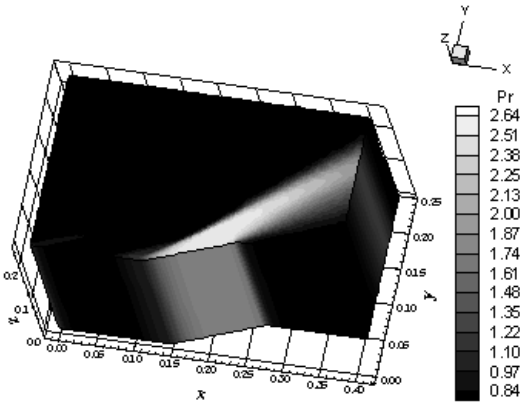

Figure 27. Pressure contours ([4]-VL).

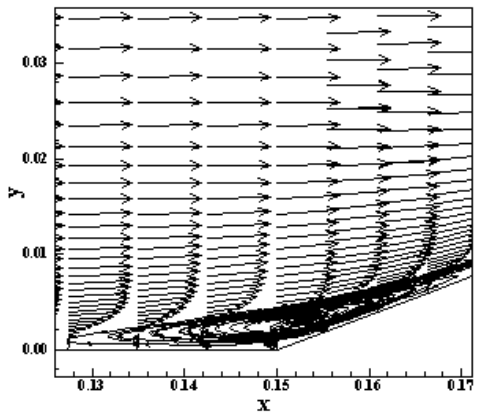

Figure 28. Streamlines and circulation bubble ([4]-VL).

Figure 33 exhibits the wall pressure distribution obtained by all three variants of the [4] TVD scheme using the [16] turbulence model. They are compared with the oblique shock wave and the

expansion wave Prandtl-Meyer theory results. All schemes detect ahead of the ramp beginning a weaker shock, which is formed due to the increase of the boundary layer thickness in this region, because of the flow separation, and the formation of the circulation bubble.

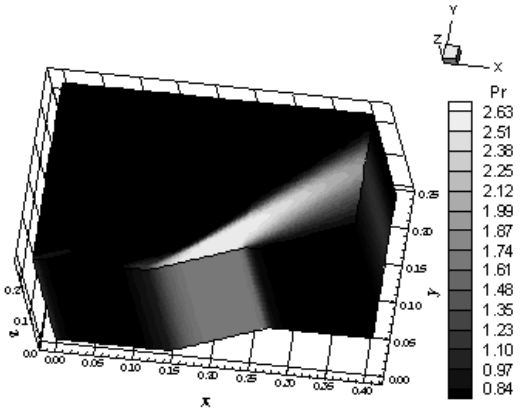

Figure 29. Pressure contours ([4]-VA).

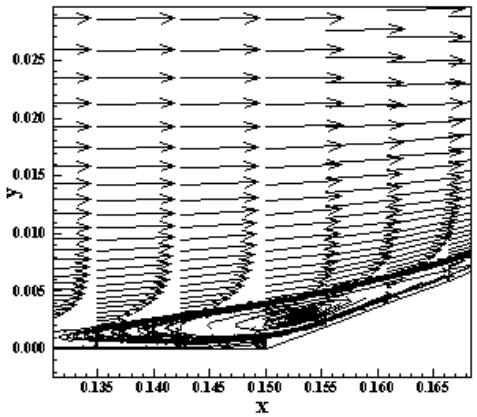

Figure 30. Streamlines and circulation bubble ([4]-VA).

As can be observed, these weaker shocks are less pronounced than the respective ones obtained in the laminar case because the effect of the turbulence model is to stabilize the boundary layer in presence of adverse pressure gradient, reducing, hence, the extension of the separation region. All three variants of the [4] TVD scheme capture the shock plateau appropriately, according to the inviscid solution, which represents a good signal of accuracy. The pressure recovery at the end of the expansion fan is well detected by all three variants of the [4] TVD scheme.

Table 10 shows the detachment and reattachment points obtained by the three limiters studied with the [4] TVD scheme using the [16] turbulence model. The [4] TVD scheme using Min limiter and the [16] model presents the minimum extent of the separation region. This region of separated flow is less extent than the respective one of the laminar results, as was recognized in those studies.

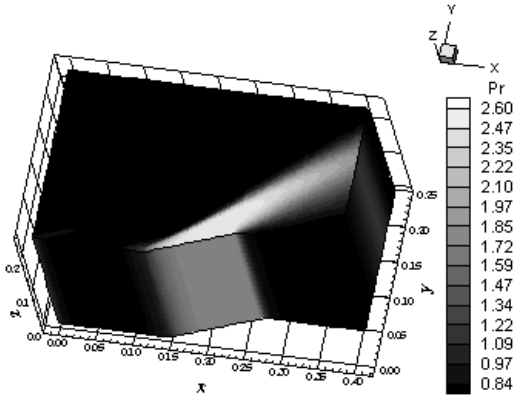

Figure 31. Pressure contours ([4]-Min).

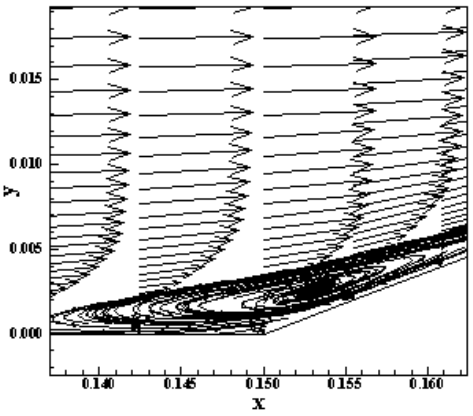

Figure 32. Streamlines and circulation bubble ([4]-Min).

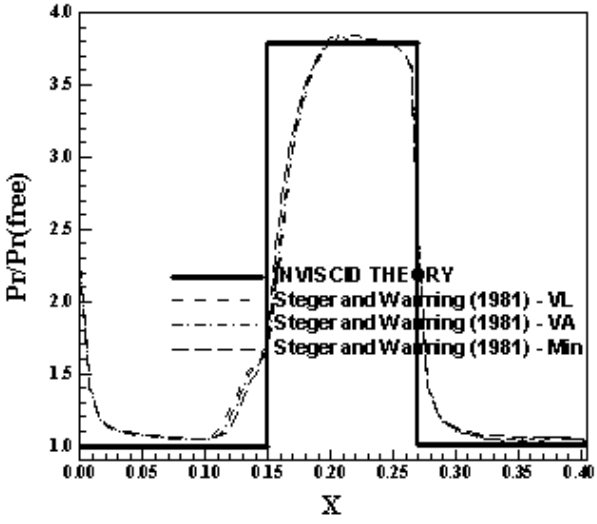

Figure 33. Wall pressure distributions ([4]-BL).

Using a transfer in Figures 27, 29 and 31, considering the xy plane, it is possible to obtain the values of the shock angle of the oblique shock wave, β, to each variant of the [4] TVD scheme using the [16] turbulence model, as well the respective errors, shown in Tab. 11. As can be observed, the [4] TVD scheme using the VA limiter and the [16] model presents the best value to the shock angle, with a percentage error of 0.27%.

Table 10. Flow separation detachment and reattachment points ([4]-Turbulent).

Scheme	Detachment (m)	Reattachment (m)
[4]-VL	0.1275	0.1718
[4]-VA	0.1276	0.1664
[4]-Min	0.1350	0.1610

Table 11. Shock angle of the oblique shock wave at the ramp and percentage error ([4]-Turbulent).

Scheme	β (°)	Error (%)
[4]-VL	38.0	0.80
[4]-VA	37.8	0.27
[4]-Min	37.1	1.59

As conclusion of the study analyzing the [4] TVD scheme in its three variants using the [16] model, the best variant is the [4] TVD scheme using VA limiter due to better accuracy in the determination of the shock angle.

Figures 34 to 37 exhibit the pressure contours and the streamlines of the velocity vector field generated by the [5] TVD scheme in two variants, namely: VA and Min, using the [16] turbulence model. The VL limiter did not present converged results. Figures 34 and 35 show the pressure contours and the streamlines, respectively, obtained by the [5] TVD scheme using VA limiter; and Figures 36 and 37 show the pressure contours and the streamlines, respectively, obtained by the [5] TVD scheme using Min limiter. The [5] TVD scheme using VA limiter yields the most severe pressure field, which characterizes the most conservative solution, involving the variants of this scheme. Good symmetry and homogeneity properties at the k planes are observed in all solutions. The shock wave is well captured. The circulation bubble is also well captured by the three limiters.

Figure 38 exhibits the wall pressure distribution obtained by the two variants of the [5] TVD scheme using the [16] turbulence model. They are compared with the oblique shock wave and the expansion wave Prandtl-Meyer theory results. All schemes detect ahead of the ramp beginning a weaker shock, which is formed due to the increase of the boundary layer thickness in this region, because of the flow separation, and the formation of the circulation bubble.

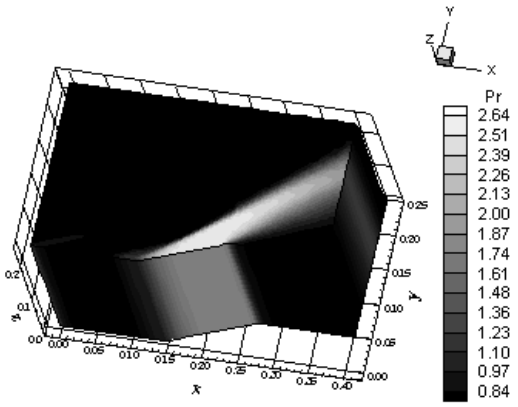

Figure 34. Pressure contours ([5]-VA).

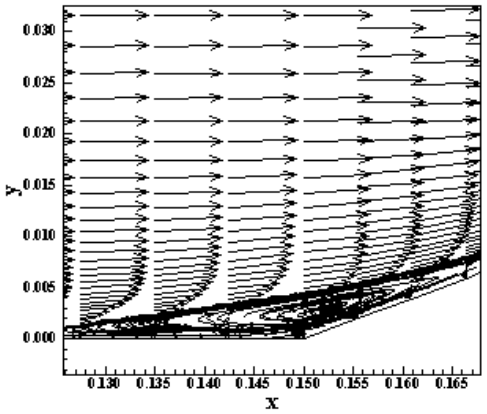

Figure 35. Streamlines and circulation bubble ([5]-VA).

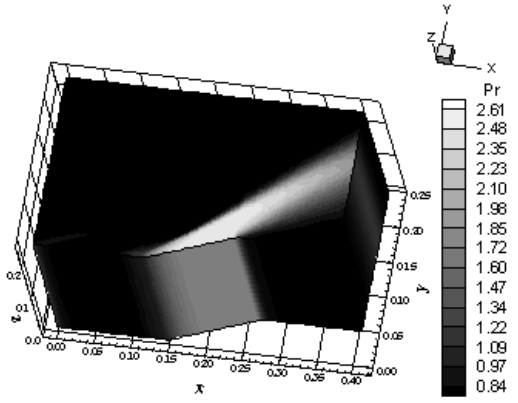

Figure 36. Pressure contours ([5]-Min).

Both variants of the [5] TVD scheme capture the shock plateau appropriately, according to the

inviscid solution, which represents a good signal of accuracy. The pressure recovery at the end of the expansion fan is well detected by both variants of the [5] TVD scheme.

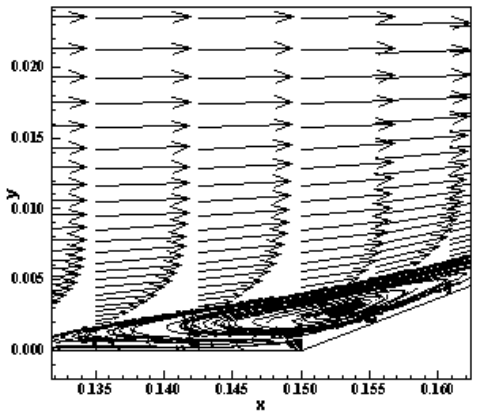

Figure 37. Streamlines and circulation bubble ([5]-Min).

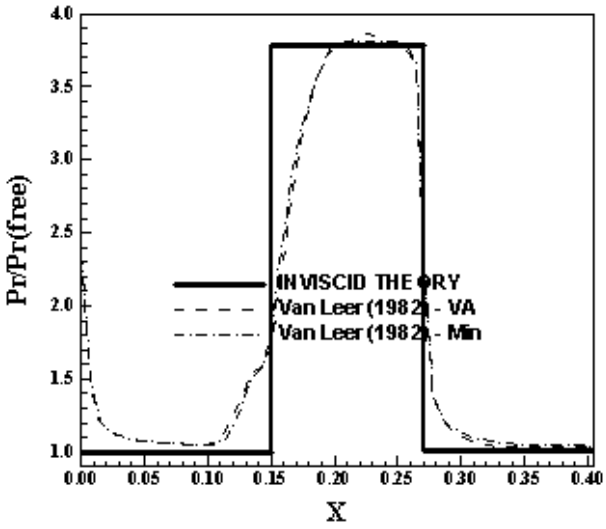

Figure 38. Wall pressure distributions ([5]-BL).

Table 12 shows the detachment and reattachment points obtained by the two limiters studied with the [5] TVD scheme, namely: VA and Min, using the [16] turbulence model. The [5] TVD scheme using Min limiter and the [16] model presents the minimum extent of the separation region. This region of separated flow is less extent than the respective one of the laminar results.

Table 12. Flow separation detachment and reattachment points ([5]-Turbulent).

Scheme	Detachment (m)	Reattachment (m)
[5]-VA	0.1275	0.1719
[5]-Min	0.1275	0.1664

Using a transfer in Figures 34 and 36, considering the xy plane, it is possible to obtain the values of the shock angle of the oblique shock wave, β, to each variant of the [5] TVD scheme using the [16] turbulence model, as well the respective errors, shown in Tab. 13. As can be observed, both variants of the [5] TVD scheme using the [16] model present the same values to the shock angle, with a percentage error of 1.86%.

Table 13. Shock angle of the oblique shock wave at the ramp and percentage error ([5]-Turbulent).

Scheme	β (°)	Error (%)
[5]-VA	37.0	1.86
[5]-Min	37.0	1.86

As conclusion of the study analyzing the [5] TVD scheme in two variants, namely: VA and Min, using the [16] model, the best variant is the [5] scheme using VA limiter due to good accuracy in the determination of the shock angle and the prediction of a more severe pressure field.

Figures 39 to 44 exhibit the pressure contours and the streamlines of the velocity vector field generated by the [6] TVD scheme in its three variants, using the [16] turbulence model. Figures 39 and 40 show the pressure contours and the streamlines, respectively, obtained by the [6] TVD scheme using VL limiter; Figures 41 and 42 show the pressure contours and the streamlines, respectively, obtained by the [6] TVD scheme using VA limiter; and Figures 43 and 44 show the pressure contours and the streamlines, respectively, obtained by the [6] TVD scheme using Min limiter.

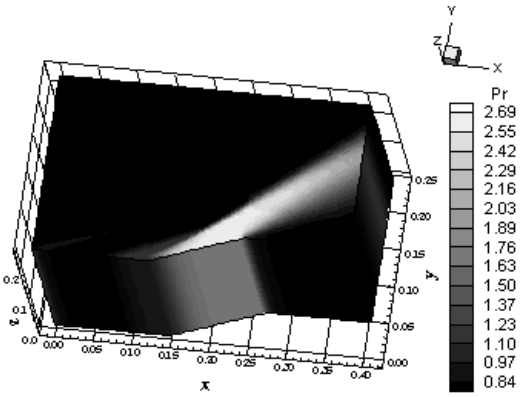

Figure 39. Pressure contours ([6]-VL).

The [6] TVD scheme using VA limiter yields the most severe pressure field, which characterizes the

most conservative solution, involving the variants of this scheme. Good symmetry and homogeneity properties at the k planes are observed in all solutions. The shock wave is well captured. The circulation bubble is also well captured by the three limiters.

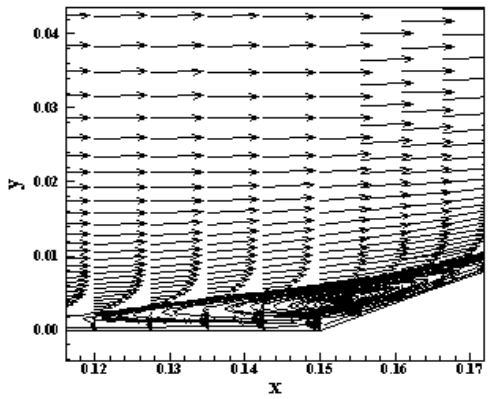

Figure 40. Streamlines and circulation bubble ([6]-VL).

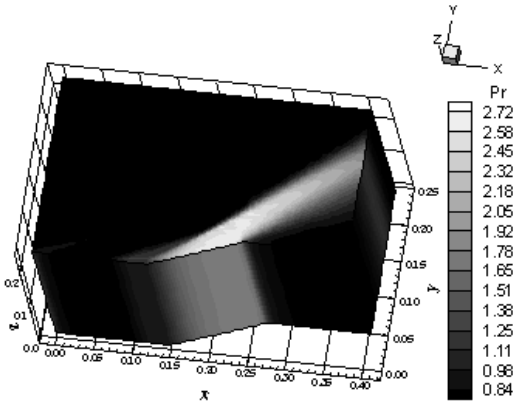

Figure 41. Pressure contours ([6]-VA).

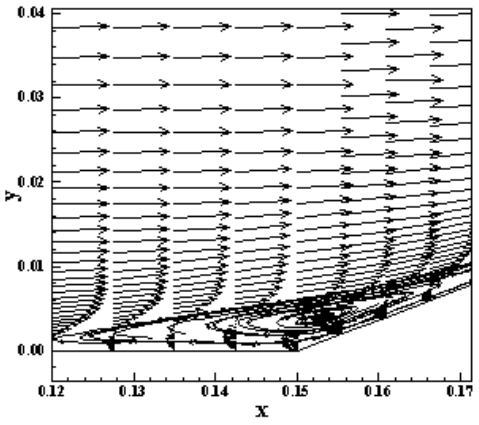

Figure 42. Streamlines and circulation bubble ([6]-VA).

Figure 45 exhibits the wall pressure distribution obtained by all three variants of the [6] TVD scheme using the [16] turbulence model. They are compared with the oblique shock wave and the expansion wave Prandtl-Meyer theory results. All schemes detect ahead of the ramp beginning a weaker shock, which is formed due to the increase of the boundary layer thickness in this region. As can be observed, these weaker shocks are as pronounced as the respective ones obtained in the laminar case;

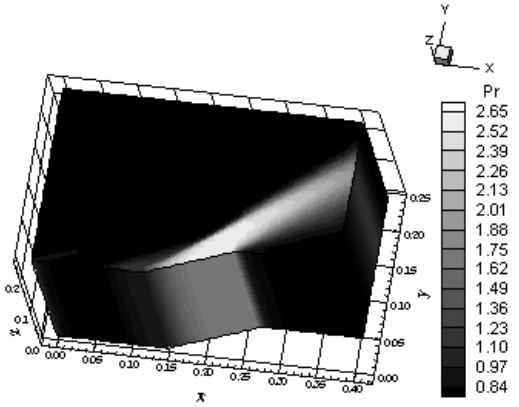

Figure 43. Pressure contours ([6]-Min).

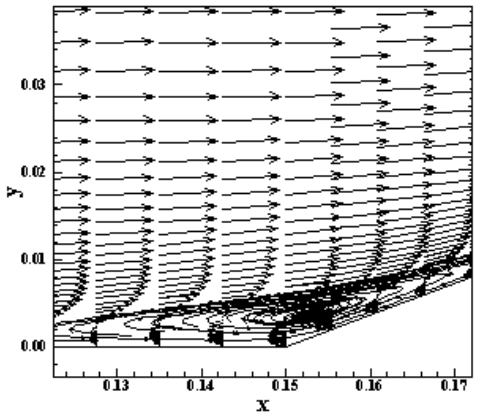

Figure 44. Streamlines and circulation bubble ([6]-Min).

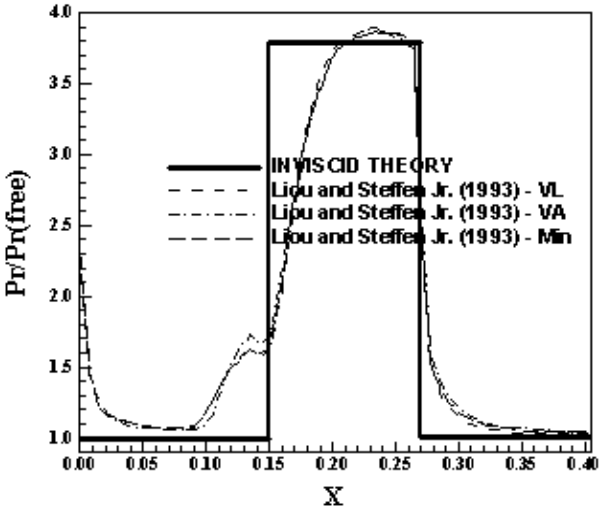

Figure 45. Wall pressure distributions ([6]-BL).

however, the effect of the turbulence model of stabilizing the boundary layer in presence of adverse pressure gradient, reducing, hence, the extension of the separation region, is well preserved, as can be seen from Tab. 14. All three variants of the [6] TVD scheme slightly over-predict the shock plateau in relation to the inviscid solution, which represents a good signal of accuracy. The pressure recovery at the end of the expansion fan is well detected by all three variants of the [6] TVD scheme.

Table 14 shows the detachment and reattachment points obtained by the three limiters studied with the [6] TVD scheme using the [16] turbulence model. The [6] TVD scheme using VL limiter and the [16] model presents the minimum extent of the separation region. This region of separated flow is less extent than the respective one of the laminar results (see [8]).

Table 14. Flow separation detachment and reattachment points ([6]-Turbulent).

Scheme	Detachment (m)	Reattachment (m)
[6]-VL	0.1126	0.1773
[6]-VA	0.1125	0.1773
[6]-Min	0.1125	0.1773

Using a transfer in Figures 39, 41 and 43, considering the xy plane, it is possible to obtain the values of the shock angle of the oblique shock wave, β, to each variant of the [6] TVD scheme using the [16] turbulence model, as well the respective errors, shown in Tab. 15. As can be observed, the [16] TVD scheme using the VA limiter and the [16] model presents the best value to the shock angle, with a percentage error of 0.53%.

Table 15. Shock angle of the oblique shock wave at the ramp and percentage error ([6]-Turbulent).

Scheme	β (°)	Error (%)
[6]-VL	37.0	1.86
[6]-VA	37.5	0.53
[6]-Min	38.0	0.80

As conclusion of the study analyzing the [6] TVD scheme in its three variants using the [16] model, the best variant is the [6] TVD scheme using VA limiter due to better accuracy in the determination of the shock angle.

Figures 46 to 51 exhibit the pressure contours and the streamlines of the velocity vector field generated by the [7] TVD scheme in its three variants, using the [16] turbulence model. Figures 46 and 47 show the pressure contours and the streamlines, respectively, obtained by the [7] TVD scheme using VL limiter; Figures 48 and 49 show the pressure contours and the streamlines, respectively, obtained by the [7] TVD scheme using VA limiter;

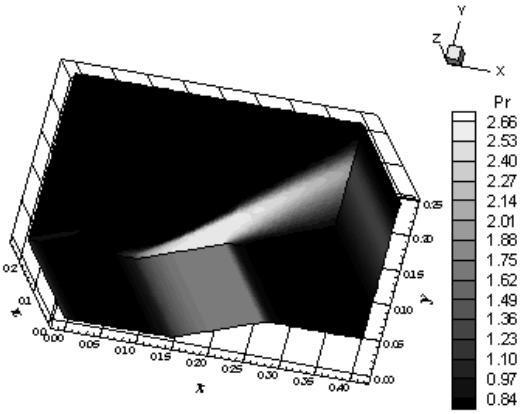

Figure 46. Pressure contours ([7]-VL).

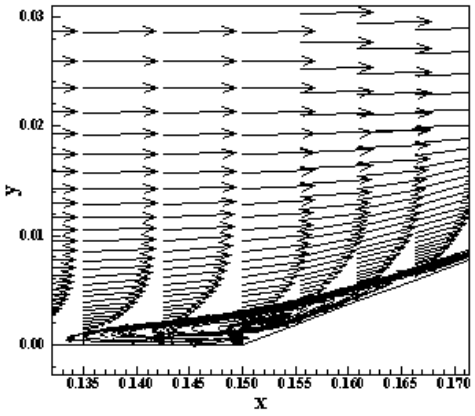

Figure 47. Streamlines and circulation bubble ([7]-VL).

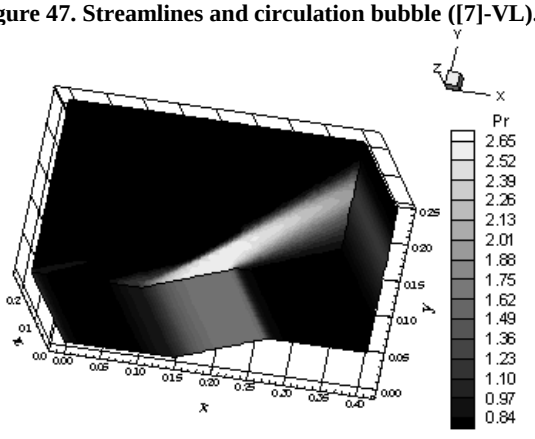

Figure 48. Pressure contours ([7]-VA).

and Figures 50 and 51 show the pressure contours and the streamlines, respectively, obtained by the

[7] TVD scheme using Min limiter. The [7] TVD scheme using VL limiter yields the most severe pressure field, which characterizes the most conservative solution, involving the variants of this scheme. Good symmetry and homogeneity properties at the k planes are observed in all solutions. The shock wave is well captured. The circulation bubble is also well captured by the three limiters.

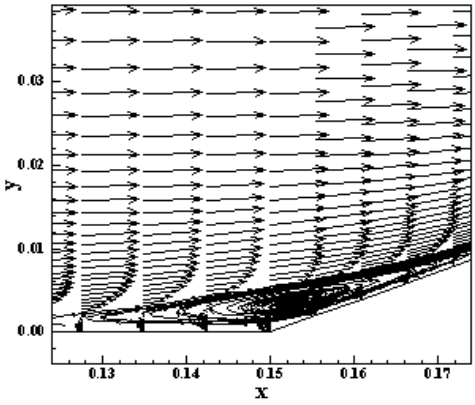

Figure 49. Streamlines and circulation bubble ([7]-VA).

Figure 52 exhibits the wall pressure distribution obtained by all three variants of the [7] TVD scheme using the [16] turbulence model. They are compared with the oblique shock wave and the expansion wave Prandtl-Meyer theory results. All schemes detect ahead of the ramp beginning a weaker shock, which is formed due to the increase of the boundary layer thickness in this region. All three variants of the [7] TVD scheme slightly over-predict the shock plateau in relation to the inviscid solution, which represents a good signal of accuracy. The pressure recovery at the end of the expansion fan is well detected by all three variants of the [7] TVD scheme.

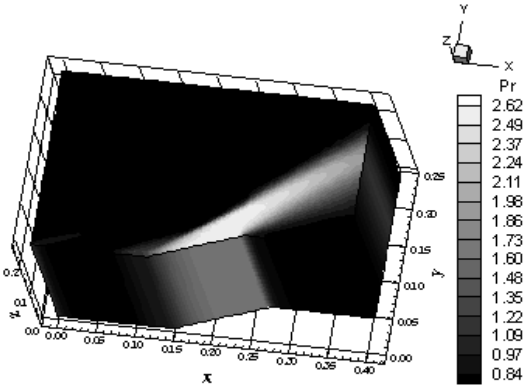

Figure 50. Pressure contours ([7]-Min).

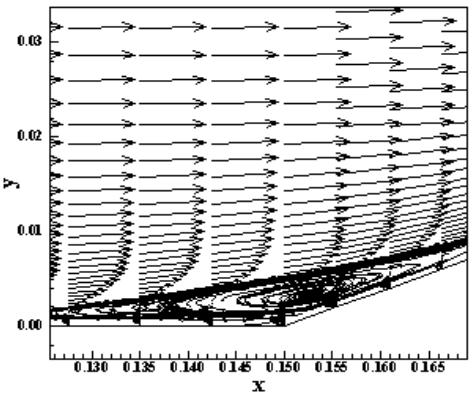

Figure 51. Streamlines and circulation bubble ([7]-Min).

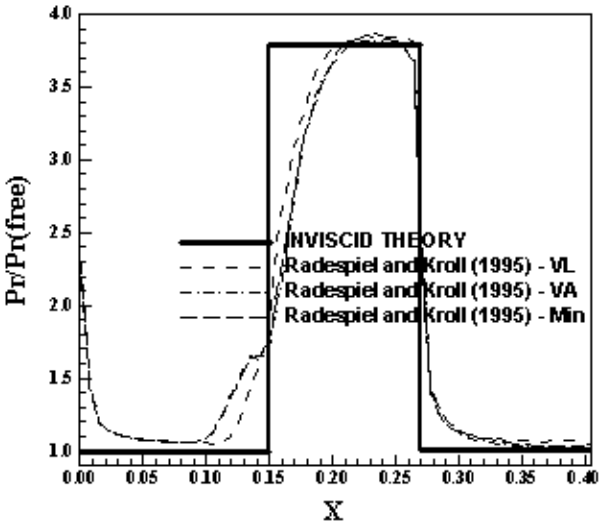

Figure 52. Wall pressure distributions ([7]-BL).

Table 16 shows the detachment and reattachment points obtained by the three limiters studied with the [7] TVD scheme using the [16] turbulence model. The [7] TVD scheme using VL limiter and the [16] model presents the minimum extent of the separation region.

Table 16. Flow separation detachment and reattachment points ([7]-Turbulent).

Scheme	Detachment (m)	Reattachment (m)
[7]-VL	0.1350	0.1664
[7]-VA	0.1200	0.1773
[7]-Min	0.1200	0.1718

Using a transfer in Figures 46, 48 and 50, considering the xy plane, it is possible to obtain the values of the shock angle of the oblique shock wave, β, to each variant of the [7] TVD scheme using the

[16] turbulence model, as well the respective errors, shown in Tab. 17. As can be observed, the results of all three limiters employed with the [7] TVD scheme using the [16] model present the same values to the shock angle, with a percentage error of 0.53%.

Table 17. Shock angle of the oblique shock wave at the ramp and percentage error ([7]-Turbulent).

Scheme	β (°)	Error (%)
[7]-VL	37.9	0.53
[7]-VA	37.5	0.53
[7]-Min	37.9	0.53

As conclusion of the study analyzing the [7] TVD scheme in its three variants using the [16] model, the best variant is the [7] TVD scheme using VL limiter due to better accuracy in the determination of the shock angle and in the determination of the most severe pressure field.

As global conclusion, the most severe pressure field using the [16] model was obtained by the [6] scheme using VA limiter, as occurred in the laminar case. The best wall pressure distributions are obtained by the [4] TVD scheme in its three variants, namely: VL, VA and Min, and by the [5] TVD scheme in its two variants, namely: VA and Min. They present pressure plateau closer to the theoretical results than the others TVD schemes. The minimum extent of the separated flow region was detected by the [4] TVD scheme using Min limiter, as occurred in the laminar case.

Table 18 - Shock angle of the oblique shock wave at the ramp and percentage error (Best Results-Turbulent).

Scheme	β (°)	Error (%)
[4]-VA	37.8	0.27
[5]-VA	37.0	1.86
[5]-Min	37.0	1.86
[6]-VA	37.5	0.53
[7]-VL	37.9	0.53
[7]-VA	37.5	0.53
[7]-Min	37.9	0.53

Table 18 presents the best values of the shock angle of the oblique shock wave obtained by each scheme. The best result of all schemes, detecting more precisely the value of the shock angle, is due to [4] TVD scheme using VA limiter. As the [4] TVD scheme has presented the best value to the shock angle of the oblique shock wave with the VA variant, the best pressure distribution in this three variants and the minimum region of separated flow with the Min limiter, the best scheme in this viscous turbulent simulation using the [16] model is due to the [4] scheme using VA and Min limiters, although the [5] in its two variants also capture good pressure distributions.

2.3 Viscous Final Conclusions

As Final conclusion, the most severe pressure field was obtained by the [6] scheme using VA limiter. This behavior was observed in the laminar case and in the turbulent cases using the [15-16] models. The best wall pressure distributions are obtained by the [4] TVD scheme in its three variants, namely: VL, VA and Min, and by the [5] TVD scheme in its two variants, namely: VA and Min, in the laminar and in the turbulent case with the [16] model. They present the pressure plateau closer to the theoretical results than the other TVD schemes. The minimum extent of the separated flow region was detected by the [4] TVD scheme using Min limiter. This was observed in the laminar as well in the turbulent cases.

Table 19. Shock angle of the oblique shock wave at the ramp and percentage error (Best Results).

Scheme	β (°)	Error (%)
[7]-Min-Lam	37.6	0.27
[6]-VL-CS	37.7	0.00
[6]-Min-CS	37.7	0.00
[4]-VA-BL	37.8	0.27

Table 19 presents the best values of the shock angle of the oblique shock wave obtained by each scheme, considering laminar and turbulent cases. The best results are due to [6] using the [15] model and the VL and Min limiters.

As the [6] TVD scheme has presented the most severe pressure field using VA limiter in all cases, laminar and turbulent, and the best value to the shock angle of the oblique shock wave with the VL and Min variants, with an error of 0.00% using the [15] model, the best final scheme is the [6] TVD scheme in its three variants.

3 Conclusions

In the present work, the [4-7] schemes are implemented, on a finite volume context and using a structured spatial discretization, to solve the Euler and the laminar/turbulent Navier-Stokes equations

in the three-dimensional space. All schemes are flux vector splitting ones and in their original implementations are first order accurate. A MUSCL approach is implemented in these schemes aiming to obtain second order spatial accuracy. The Van Leer, the Van Albada and the Minmod nonlinear limiters are employed to guarantee such accuracy and TVD high resolution properties. These flux vector splitting schemes employ approximate factorizations in ADI form to solve implicitly the Euler equations. To solve the laminar/turbulent Navier-Stokes equations, an explicit formulation based on a dimensional splitting procedure is employed. All schemes are first order accurate in time in their implicit and explicit versions. Turbulence is taken into account considering two algebraic models, namely: the [14-15] ones. The algorithms are accelerated to the steady state solution using a spatially variable time step, which has demonstrated effective gains in terms of convergence rate ([20-21]. All four schemes are applied to the solution of the physical problems of the supersonic flow along a compression corner, in the inviscid case, and of the supersonic flow along a ramp, in the laminar and turbulent cases. The results have demonstrated that the most severe and most accurate results are obtained with the [6] TVD high resolution scheme.

In the implicit inviscid case, the most severe pressure field was obtained by the [6] scheme using VA limiter. The best wall pressure distributions obtained by each scheme is shown in [8]. The best wall pressure distribution among the distributions presented is due to [6] using Min limiter. [8] also presents the best values of the shock angle of the oblique shock wave obtained by each scheme. Except the [4] TVD scheme, all others schemes always present a variant with the correct value of the shock angle. As the [6] TVD scheme has presented the best wall pressure distribution using Min limiter and as it also presents the correct value of the shock angle of the oblique shock wave with this variant (the other two limiters too), the best scheme in the inviscid simulation is due to the [6] scheme using Min limiter.

In the viscous case, the most severe pressure field was obtained by the [6] scheme using VA limiter. This behavior was observed in the laminar case and in the turbulent cases using the [15-16] models. The best wall pressure distributions are obtained by the [4] TVD scheme in its three variants, namely: VL, VA and Min, and by the [5] TVD scheme in its two variants, namely: VA and Min, in the laminar and in the turbulent case with the [16] model. They present the pressure plateau closer to the theoretical results than the other TVD schemes. The minimum extent of the separated flow region was detected by the [4] TVD scheme using Min limiter. This was observed in the laminar as well in the turbulent cases.

Table 19 presents the best values of the shock angle of the oblique shock wave obtained by each scheme, considering laminar and turbulent cases. The best results are due to [6] using the [15] model and the VL and Min limiters.

As the [6] TVD scheme has presented the most severe pressure field using VA limiter in all cases, laminar and turbulent, and the best value to the shock angle of the oblique shock wave with the VL and Min variants, with an error of 0.00% using the [15] model, the best final scheme is the [6] TVD scheme in its three variants.

As final conclusion, the present author recommends the [6] TVD scheme, due to the best performance in the inviscid and viscous laminar and turbulent cases, to obtain more severe and accurate solutions in the three-dimensional space, which are desirable properties to the design and experimental phases of aerospace vehicles.

4 Acknowledgments

The present author acknowledges the CNPq by the financial support conceded under the form of a DTI (Industrial Technological Development) scholarship no. 384681/2011-5. He also acknowledges the infra-structure of the ITA that allowed the realization of this work.

References:

[1] P. Kutler, Computation of Three-Dimensional, Inviscid Supersonic Flows, *Lecture Notes in Physics*, Springer Verlag, Berlin, Vol. 41, 1975, pp. 287-374.

[2] J. L. Steger, Implicit Finite-Difference Simulation of Flow About Arbitrary Two-Dimensional Geometries, *AIAA Journal*, Vol. 16, No. 7, 1978, pp. 679-686.

[3] P. L. Roe, Approximate Riemann Solvers, Parameter Vectors, and Difference Schemes, *Journal of Computational Physics*, Vol. 43, 1981, 357-372.

[4] J. L. Steger, R. F. Warming, Flux Vector Splitting of the Inviscid Gasdynamic Equations with Application to Finite-Difference Methods,

Journal of Computational Physics, Vol. 40, 1981, pp. 263-293.

[5] B. Van Leer, Flux-Vector Splitting for the Euler Equations, *Lecture Notes in Physics*, Vol. 170, 1982, pp. 507-512, Springer Verlag, Berlin.

[6] M. Liou, C. J. Steffen Jr., A New Flux Splitting Scheme, *Journal of Computational Physics*, Vol. 107, 1993, pp. 23-39.

[7] R. Radespiel, N. Kroll, Accurate Flux Vector Splitting for Shocks and Shear Layers, *Journal of Computational Physics*, Vol. 121, 1995, pp. 66-78.

[8] E. S. G. Maciel, TVD Flux Vector Splitting Algorithms Applied to the Solution of the Euler and Navier-Stokes Equations in Three-Dimensions – Part I, WSEAS Transactions on Fluid Mechanics (under revision).

[9] C. Hirsch, *Numerical Computation of Internal and External Flows – Computational Methods for Inviscid and Viscous Flows*, John Wiley & Sons Ltd, 691p, 1990.

[10] R. M. Beam, R. F. Warming, An Implicit Factored Scheme for the Compressible Navier-Stokes Equations, *AIAA Journal*, Vol. 16, No. 4, 1978, pp. 393-402.

[11] J. Douglas, On the Numerical Integration of $u_{xx}+u_{yy}=u_t$ by Implicit Methods, *Journal of the Society of Industrial and Applied Mathematics*, Vol. 3, 1955, pp. 42-65.

[12] D. W. Peaceman, H. H. Rachford, The Numerical Solution of Parabolic and Elliptic Differential Equations, *Journal of the Society of Industrial and Applied Mathematics*, Vol. 3, 1955, pp. 28-41.

[13] J. Douglas, J. E. Gunn, A General Formulation of Alternating Direction Methods, *Numerische Mathematiks*, Vol. 6, 1964, pp. 428-453.

[14] N. N. Yanenko, *The Method of Fractional Steps*, Springer Verlag, NY, EUA, 1971.

[15] T. Cebeci, A. M. O. Smith, A Finite-Difference Method for Calculating Compressible Laminar and Turbulent Boundary Layers, *Journal of Basic Engineering*, Trans. ASME, Series B, Vol. 92, No. 3, 1970, pp. 523-535.

[16] B. D. Baldwin, H. Lomax, Thin Layer Approximation and Algebraic Model for Separated Turbulent Flows, *AIAA Paper 78-257*, 1978.

[17] E. S. G. Maciel, Turbulent Flow Simulations Using the MacCormack and the Jameson and Mavriplis Algorithms Coupled with the Cebeci and Smith and the Baldwin and Lomax Models in Three-Dimensions, *Engineering Applications of Computational Fluid Mechanics*, China, Vol. 1, No. 3, 2007, pp. 147-163.

[18] R. W. MacCormack, The Effect of Viscosity in Hypervelocity Impact Cratering, *AIAA Paper 69-354*, 1969.

[19] A. Jameson, D. J. Mavriplis, Finite Volume Solution of the Two-Dimensional Euler Equations on a Regular Triangular Mesh, *AIAA Journal* Vol. 24, No. 4, 1986, pp. 611-618.

[20] E. S. G. Maciel, Analysis of Convergence Acceleration Techniques Used in Unstructured Algorithms in the Solution of Aeronautical Problems – Part I, *Proceedings of the XVIII International Congress of Mechanical Engineering (XVIII COBEM)*, Ouro Preto, MG, Brazil, 2005. [CD-ROM]

[21] E. S. G. Maciel, Analysis of Convergence Acceleration Techniques Used in Unstructured Algorithms in the Solution of Aerospace Problems – Part II, *Proceedings of the XII Brazilian Congress of Thermal Engineering and Sciences (XII ENCIT)*, Belo Horizonte, MG, Brazil, 2008. [CD-ROM]

[22] R. W. Fox, A. T. McDonald, *Introdução à Mecânica dos Fluidos*, Ed. Guanabara Koogan, Rio de Janeiro, RJ, Brazil, 632p, 1988.

[23] J. D. Anderson Jr., *Fundamentals of Aerodynamics*, McGraw-Hill, Inc., EUA, 563p, 1984.